International Journal of Thermophysics, Vol. 24, No. 5, September 2003 (© 2003)

Numerical Simulation of Heat Conduction to Liquids from a Thin Vertical Cylinder[1]

F. Gori[2, 3] and M. G. Serranò[2]

The paper presents numerical simulations of heat conduction around a circular vertical cylinder immersed in liquids. A finite volume formulation is used, and the numerical analysis is performed in unsteady state with an explicit scheme. The numerical predictions are compared with experiments performed on liquids to find the temperature inside the cylinder, where a thermocouple is located, and at the wall of the insulated coaxial container, where the liquid is poured. The cylinder is immersed vertically. The numerical results are in good agreement with the temperature at the wall of the container. The experimental temperature measurement of the thermocouple located inside the probe is intermediate between the numerical temperatures on the axis and on the surface of the probe. The natural convection phenomenon is evidenced in the experiments, after a certain time from the beginning of heating, in some of the liquids used, except glycerol. Natural convection is not considered in the present numerical simulations, which solve only the heat conduction equation.

KEY WORDS: finite volume method; heat conduction; liquids; numerical simulation; thin cylinder.

1. INTRODUCTION

The thermal probe is an instrument used to measure the thermal conductivity of liquids and porous granular materials, as established by Blackwell [1],

[1] Paper presented at the Sixteenth European Conference on Thermophysical Properties, September 1–4, 2002, London, United Kingdom.

[2] Department of Mechanical Engineering, University of Rome "Tor Vergata" via del Politecnico 1, 00133 Rome, Italy.

[3] To whom correspondence should be addressed. E-mail: gori@uniroma2.it

0195-928X/03/0900-1325/0 © 2003 Plenum Publishing Corporation

Jaeger [2], De Vries and Peck [3], and reported by Carslaw and Jaeger [4]. The probe construction is a very difficult laboratory task, because the design of the internal parts of the probe can introduce some significant limitations on uncertainties [5].

Several probes have been constructed in the laboratories of the first author of this work [6–12]. A common guideline in the correct construction of the thermal probe is to have a length-to-diameter ratio of the probe greater or equal to 100. In several cases, geometrical restrictions do not allow to have such a high ratio, and, in these cases, it is desirable to have a numerical approach that could help in the evaluation of the errors and in the proper design of the probe.

The present paper reports numerical simulations of heat conduction to liquids from a heated thin vertical cylinder, which is used as a thermal probe.

2. NUMERICAL SIMULATION

2.1. Geometry and Physical Properties

The thermal probe, constructed in the Laboratory of Heat Transfer of the University of Rome "Tor Vergata," has been described in Refs. 13 and 14. It is composed of a hollow stainless steel cylinder, with a length of 59.5 mm, an external diameter of 0.6 mm, and an internal diameter of 0.3 mm, containing a platinum heating wire, with an electrical resistance of 5.8 Ω and a diameter of 65 μm, and a thermocouple made of two copper—constantan wires, 76 μm in diameter. An epoxy resin, poured inside the cylinder in the liquid state, helps to maintain the stability of the heating wire and the thermocouple after its solidification. The handle of the probe is made with the same epoxy resin. The thermocouple junction is located at the middle of the probe.

In the numerical simulations the thermal probe has been assumed to be composed of an inner cylinder, made of epoxy resin, with a radius of 0.15 mm and an outer steel annulus of radius 0.3 mm. The epoxy resin has the following physical properties, density of 1250 $kg \cdot m^{-3}$, specific heat of 1045 $J \cdot kg^{-1} \cdot K^{-1}$, and a thermal conductivity of 0.2 $W \cdot m^{-1} \cdot K^{-1}$. The properties of the stainless steel are: density of 7820 $kg \cdot m^{-3}$, specific heat of 460 $J \cdot kg^{-1} \cdot K^{-1}$, and a thermal conductivity of 14 $W \cdot m^{-1} \cdot K^{-1}$, as found from the literature.

The numerical simulation assumes the fluid is set in a cylindrical container (diameter of 48 mm) with insulated boundaries and the thermal probe is maintained vertically on the axis.

2.2. Equations

The thermal probe is step-heated by direct electric current, and the power is generated on the axis of the probe. The temperature distribution in the probe and in the heated liquid is determined from the numerical solution of the heat conduction equation,

$$\rho c \frac{\partial T}{\partial t} = \lambda \left[\frac{1}{r} \frac{\partial}{\partial r} \left(r \frac{\partial T}{\partial r} \right) + \frac{\partial^2 T}{\partial z^2} \right] + q \tag{1}$$

where ρ, c, λ are the density, specific heat, and thermal conductivity of the medium, respectively, T and t are the temperature and the time, respectively, r and z are the radial and axial co-ordinates, and q is the heat power for a volume unit.

Equation (1) has been solved numerically using the finite volume technique, according to Ref. 15. With the time explicit scheme, Eq. (1) becomes

$$a_{P1} T_P(t+\Delta t) = a_P T_P(t) + a_W T_W(t) + a_E T_E(t) + a_S T_S(t) + a_N T_N(t) + S \tag{2}$$

where the coefficients are relative to Fig. 1, according to the method of Ref. 15. The term S in Eq. (2) can take into account the heat generated within the entire volume of the thermal probe or on the axis of the probe.

2.3. Grids

The first grid used is made dividing the physical region, in the radial direction from the axis of the probe to the container wall, into 58 parts, with $\Delta r = 0.15$ mm inside the probe and $\Delta r = 0.42$ mm in the fluid. In this

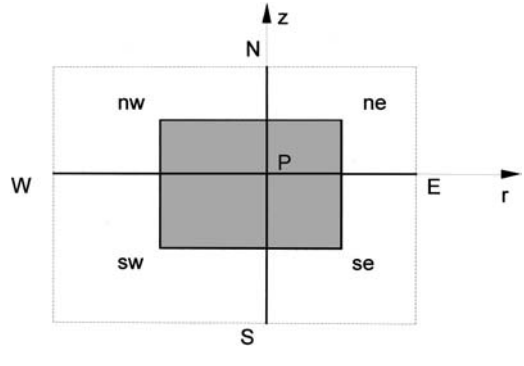

Fig. 1. Control volume.

way, three nodes of the grid are inside the probe. The first one is on the axis, the second at the boundary between epoxy resin and steel, and the third one at the surface boundary between steel and liquid. The physical region in the axial direction has been divided into 161 nodes, of length $\Delta z = 0.4375$ mm.

In a numerical explicit scheme the time step is normally a function of the grid size. The present numerical analysis has found it convenient to assume the time step to be given by

$$\Delta t = \frac{\Delta x_{\min}^2}{5\alpha_{\max}} \tag{3}$$

where $\Delta x_{\min}$ is the minimum value of the grid space and $\alpha_{\max}$ is the maximum value of the thermal diffusivity of the materials involved in the calculations.

The grid independence test has been done comparing the results of the first grid with those of a second grid, made with 115 nodes in the radial direction (with $\Delta r = 0.15$ mm inside the probe and $\Delta r = 0.21$ mm in the liquid) and 321 nodes in the axial direction (with $\Delta z = 0.21$ mm).

2.4. Uncertainty Estimate

The uncertainty in the numerical solutions, or grid independence test, has been evaluated by comparing the numerical results obtained with the two grids described in the previous chapter. The temperature difference of the numerical solutions, obtained with the two grids, is never higher than 0.07 K.

The numerical simulation is possible only by assuming an input value of the thermal conductivity of the investigated liquid. On the other hand, the method of the perfect line source can be used to calculate the thermal conductivity by the slope of the temperature increase, on a semi-logarithmic scale versus time, according to the well known relation, in dimensionless form [4],

$$\Delta T^* = 0.5(\ln 4t^* - 0.5772), \tag{4}$$

also known as the perfect line source (PLS) solution.

In other words, the temperature values, obtained by the numerical analysis, have been reported, as a function of time, on a semi-logarithmic scale, and the thermal conductivity has been evaluated with the method of the perfect line source. The difference between the input value of the numerical analysis and the value obtained by the slope of the curve has

been found to be smaller than 4% in all cases, except for silicon oil where the difference is 6%.

The experimental uncertainty analysis has been reported in detail in Refs. 13 and 14, and is not repeated in the present paper, where the main concern is the numerical analysis. The experimental temperature uncertainty has been found to be less than 0.1°C. The standard uncertainty in the measurement of the temperature has been analyzed with the residuals and is generally less than 0.03°C. Uncertainties propagation from measurements of the current supplied by the feeder and of the variation in the power due to the increase of the heater resistance, along with the uncertainty in the diameter and length of the heater, resulted in an overall uncertainty in thermal conductivity of between 1 and 2%.

The presence of natural convection in the experiments is not taken into consideration by the numerical analysis because the evaluation of the slope of the curve is carried out only in the linear region and before the onset of natural convection.

3. COMPARISON BETWEEN NUMERICAL SIMULATIONS AND EXPERIMENTAL RESULTS

The experiments, carried out in the Heat Transfer Laboratory, are reported in detail in Refs. 13 and 14.

3.1. Glycerol

Several liquids have been investigated numerically. The first one is glycerol because it is commonly used as a reference liquid for the calibration of the thermal probe. The temperature increase in glycerol is reported in Fig. 2, on a semi-logarithmic scale, in dimensional form. The numerical simulation has been carried out from 1 s to about 2000 s and the temperature increase can be, at maximum, 5.2 K higher than the initial value. The highest temperature increase has been calculated numerically on the axis, curve 1, and is variable from 1 K to about 5.2 K at 2000 s. The temperature difference at the steel surface, curve 2, is almost 2 K lower than on the axis, and it increases from about 0.4 K at 1 s to about 3.1 K at 2000 s. Finally, the temperature increase at the wall of the cylindrical container, curve 3, due to the overall heating of the liquid, has been predicted, and Fig. 2 shows that the increase is almost zero up to 1000 s and it is only equal to 0.3 K at 2000 s.

The numerical predictions appear in good agreement with the experiments. The experimental increase in temperature of the thermocouple

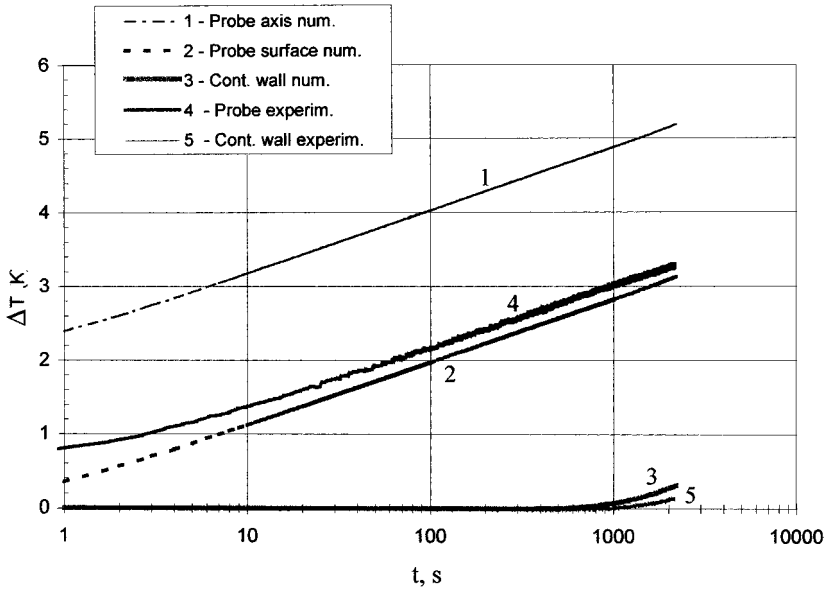

Fig. 2. Dimensional temperature increase in glycerol. Curves 1, 2, and 3 are numerical predictions, where curve 1 is relative to the probe axis, curve 2 to the probe surface, and curve 3 to the temperature on the wall of the container. Curves 4 and 5 are experimental measurements where curve 4 is relative to the thermocouple in the probe and curve 5 to the container wall.

inside the probe, curve 4, is intermediate between the numerical value on the axis and that on the surface. This is really a good comparison because the thermocouple is located internally at the probe but the exact position is very difficult to be detected. The experimental increase in temperature, at the wall of the container, curve 5, is almost equal to the numerical prediction.

The numerical predictions in glycerol, with the two numerical grids described previously, have shown a maximum temperature difference of 0.07 K. The numerical data of Fig. 2 have been used to calculate the thermal conductivity of glycerol, and the difference between the initial value ($0.274\ W \cdot m^{-1} \cdot K^{-1}$) and the value calculated by the numerical results is 1.2%.

The numerical predictions for glycerol are reported in Fig. 3, in dimensionless form, along with the experiments and the PLS (perfect line source) solution, curve 2. Good agreement is observed between the PLS solution and the numerical results on the wall of the steel, almost coincident to each other, curve 2. Figure 3 presents the dimensionless numerical

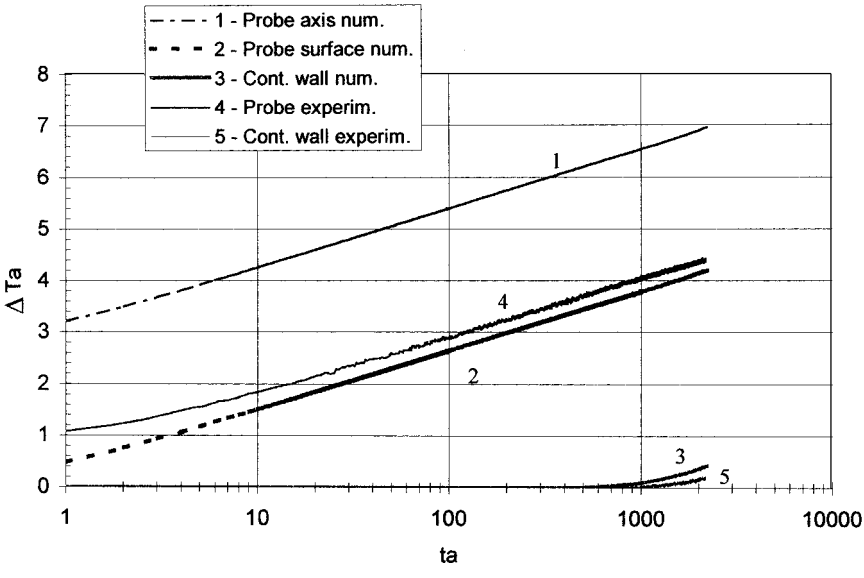

Fig. 3. Dimensionless temperature increase in glycerol. Curves 1, 2, and 3 are numerical predictions, where curve 1 is relative to the probe axis, curve 2 to the probe surface, and curve 3 to the temperature on the wall of the container. Curve 2 also represents the PLS (perfect line solution) coincident with the numerical solution on the probe surface. Curves 4 and 5 are experimental measurements where curve 4 is relative to the thermocouple in the probe and curve 5 to the container wall.

temperature increase, versus the dimensionless time, on the axis, on the external surface of the thermal probe, and on the container wall.

Figure 3 reports also the experimental temperatures measured by the thermocouple, which is present inside the thermal probe, and the experimental temperatures of the thermocouple located on the cylindrical wall of the container. The temperature on the container wall remains almost constant during the measurements showing that the assumption of an infinite container is well approximated by the experiments. The experimental data fall within the predictions for the surface and the axis of the thermal probe. Reasonable agreement is found with the predictions obtained on the surface.

3.2. Water

The second liquid investigated is water and the numerical, as well as the experimental results, are presented in Figs. 4 and 5, respectively, in dimensional and dimensionless forms. The numerical predictions of Fig. 4

show a continuous increase of the temperature difference, according to the heat conduction equation used in the numerical simulation, while, the real experiment shows that, after about 23 s, the water starts to develop natural convection (curve 4). The experimental temperature is almost constant up to about 163 s, when a temperature increase is present (corresponding to 1.9 K), because of the overall heating of the water, as confirmed by the increase of the temperature at the wall of the container (curve 5). The numerical simulation at the wall of the container (curve 3) is in good agreement with the experimental results, and they start to increase after about 163 s. The numerical simulation on the axis (curve 1) gives a higher temperature than the other temperatures. The numerical simulation on the wall of the probe (curve 2) gives a lower temperature than the experimental result for the probe thermocouple (curve 4), and also this result is justified by the fact that the probe is located inside the cylinder and a layer of epoxy layer is present. The numerical temperature difference, obtained with the two grids, has been found to be less than 0.06 K and the thermal conductivity, evaluated by the numerical solution, has been found different from the input value ($0.66\ W \cdot m^{-1} \cdot K^{-1}$) by 3.6%.

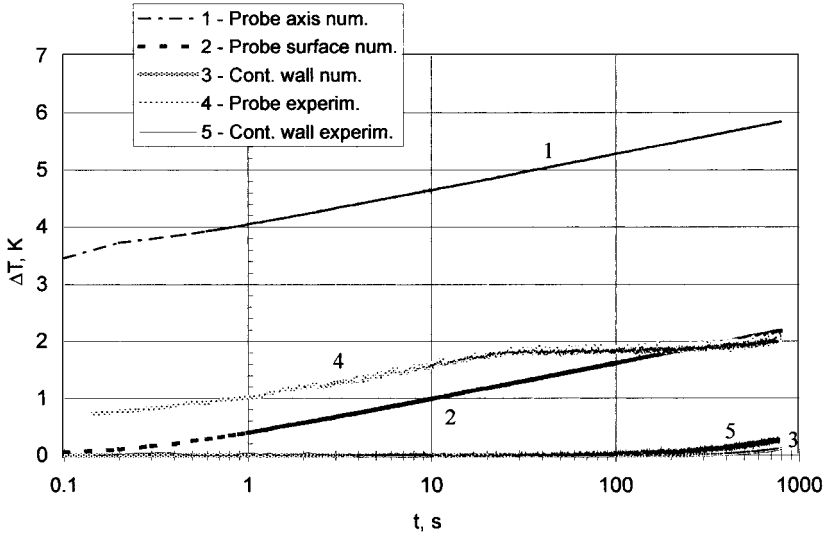

Fig. 4. Dimensional temperature increase in water. Curves 1, 2, and 3 are numerical predictions, where curve 1 is relative to the probe axis, curve 2 to the probe surface, and curve 3 to the temperature on the wall of the container. Curves 4 and 5 are experimental measurements where curve 4 is relative to the thermocouple in the probe and curve 5 to the container wall.

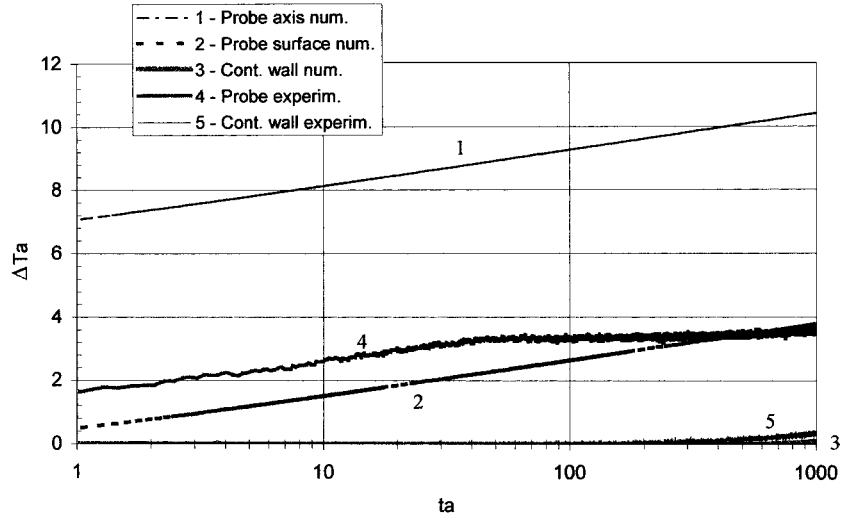

Fig. 5. Dimensionless temperature increase in water. Curves 1, 2, and 3 are numerical predictions, where curve 1 is relative to the probe axis, curve 2 to the probe surface, and curve 3 to the temperature on the wall of the container. Curve 2 also represents the PLS (perfect line solution) coincident with the numerical solution on the probe surface. Curves 4 and 5 are experimental measurements where curve 4 is relative to the thermocouple in the probe and curve 5 to the container wall.

The dimensionless results, reported in Fig. 5, show that the numerical temperature on the probe surface (curve 2) is almost coincident with the PLS solution.

3.3. Ethylene Glycol

The results of the numerical simulations with ethylene glycol are reported in Figs. 6 and 7 in dimensional and dimensionless form, respectively. Considerations for Fig. 6 are similar to the previous ones with water, Fig. 4. In ethylene glycol, natural convection starts after 84 s. Numerical predictions on the probe surface (curve 2) are in agreement with the experiments (curve 4) from the beginning of heating, with a temperature difference that is constant up to the occurrence of natural convection. The temperature difference of the numerical predictions, obtained with the two grids, is less than 0.06 K, and the thermal conductivity, evaluated by the slope of the numerical results, is 3.6% different from the input value ($0.252\,W \cdot m^{-1} \cdot K^{-1}$).

Figure 6 shows good agreement between numerical predictions and experiments at the wall of the container (curves 3 and 5) and between the

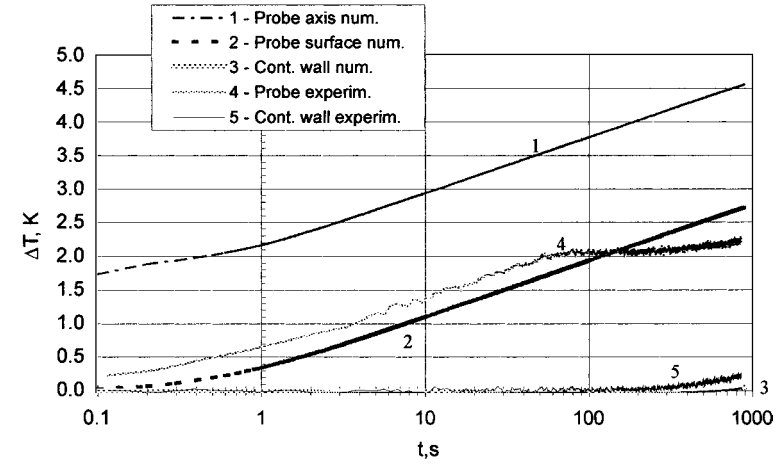

Fig. 6. Dimensional temperature increase in etylene glicol. Curves 1, 2, and 3 are numerical predictions, where curve 1 is relative to the probe axis, curve 2 to the probe surface, and curve 3 to the temperature on the wall of the container. Curves 4 and 5 are experimental measurements where curve 4 is relative to the thermocouple in the probe and curve 5 to the container wall.

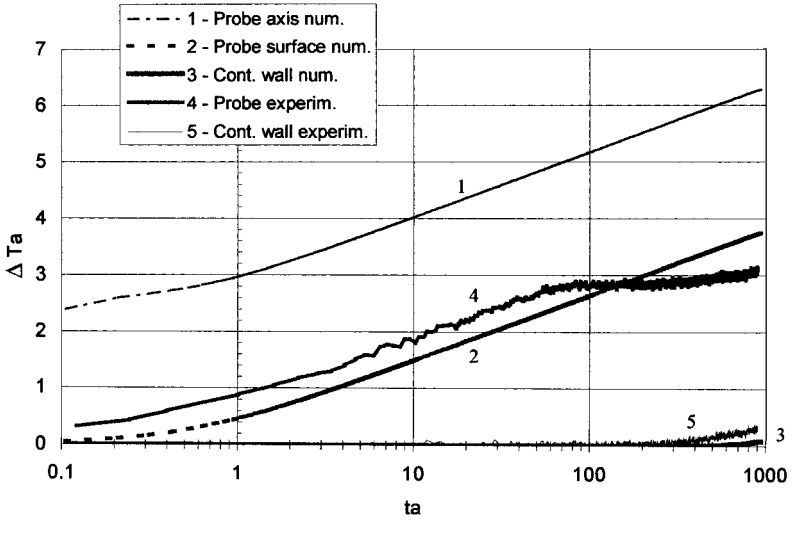

Fig. 7. Dimensionless temperature increase in etylene glicol. Curves 1, 2, and 3 are numerical predictions, where curve 1 is relative to the probe axis, curve 2 to the probe surface, and curve 3 to the temperature on the wall of the container. Curve 2 also represents the PLS (perfect line solution) coincident with the numerical solution on the probe surface. Curves 4 and 5 are experimental measurements where curve 4 is relative to the thermocouple in the probe and curve 5 to the container wall.

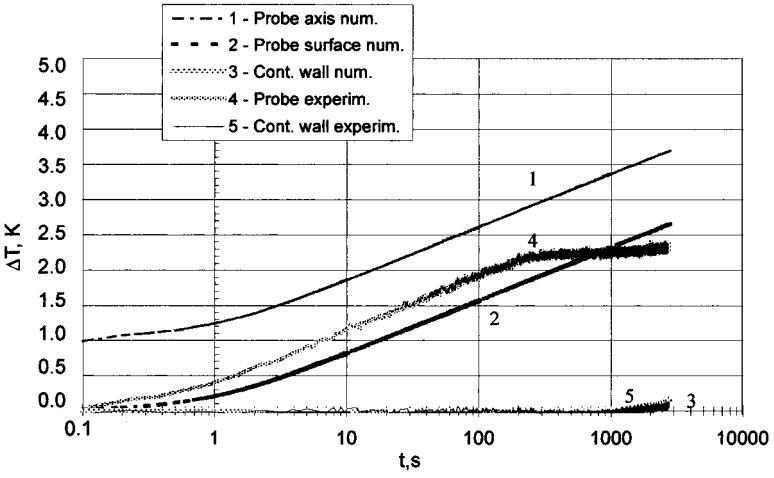

Fig. 8. Dimensional temperature increase in silicon oil. Curves 1, 2, and 3 are numerical predictions, where curve 1 is relative to the probe axis, curve 2 to the probe surface, and curve 3 to the temperature on the wall of the container. Curves 4 and 5 are experimental measurements where curve 4 is relative to the thermocouple in the probe and curve 5 to the container wall.

probe wall and the probe thermocouple (curves 2 and 4). Furthermore, the numerical predictions are in good agreement with the PLS solutions (curve 2), coincident and superimposed in Fig. 7.

3.4. Silicon Oil

The last liquid investigated here is silicon oil. Figures 8 and 9 present the dimensional and dimensionless temperature increases. In silicon oil natural convection starts after 197 s. Agreement is again good. The numerical temperature difference, obtained with the two grids, is less than 0.06 K and the thermal conductivity difference, between the input value and that evaluated by the slope, is 6%.

4. CONCLUSIONS

The numerical procedure used for the simulations has provided good agreement between predictions and experiments. The grid independence test has been satisfied giving temperature differences of less than 0.1 K between the two numerical results. The method of the perfect line source

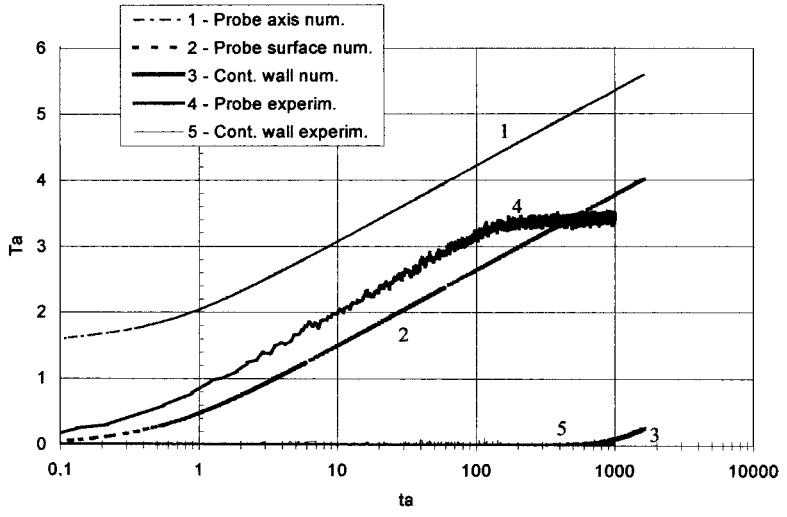

Fig. 9. Dimensionless temperature increase in silicon oil. Curves 1, 2, and 3 are numerical predictions, where curve 1 is relative to the probe axis, curve 2 to the probe surface, and curve 3 to the temperature on the wall of the container. Curve 2 also represents the PLS (perfect line solution) coincident with the numerical solution on the probe surface. Curves 4 and 5 are experimental measurements where curve 4 is relative to the thermocouple in the probe and curve 5 to the container wall.

evaluation of the thermal conductivity, from the slope of the numerical results on a semi-logarithmic scale, can provide confirmation of the value used as an input parameter in the numerical analysis. For the liquids investigated, the difference between input and final values is less than 3.6%, except for silicon oil which is 6%. Good agreement has been found between numerical predictions at the probe surface and the probe thermocouple, whose value is somewhat higher because of the temperature drop across the epoxy resin layer inside the probe.

NOMENCLATURE

a coefficient (Eq. (2)), $W \cdot K^{-1}$
c specific heat, $J \cdot kg^{-1} \cdot K^{-1}$
D probe diameter, m
q heat power, W
r radial co-ordinate, m
S heat generation term (Eq. (2)), W

T	temperature, K
T^*	$\alpha T/(D/2)^2$ dimensionless temperature
t	time, s
t^*	$2\pi\lambda\Delta T/q$ dimensionless time
x	grid length, m
z	axial co-ordinate, m

Greek

α	thermal diffusivity, $m^2 \cdot s^{-1}$
λ	thermal conductivity, $W \cdot m^{-1} \cdot K^{-1}$
ρ	density, $kg \cdot m^{-3}$
Δ	increment

Subscript

a	dimensionless quantity
max	maximum value
min	minimum value
P	point P (Fig. 1)
W	point W (Fig. 1)
E	point E (Fig. 1)
S	point S (Fig. 1)
N	point N (Fig. 1)

Superscript

*	non-dimensional quantity

ACKNOWLEDGMENTS

The authors thank ASI (Agenzia Spaziale Italiana) for partial financial support. The authors thank Dr. G. Foschi for help given during the preparation of the manuscript.

REFERENCES

1. J. H. Blackwell, *J. Appl. Phys.* **25**:137 (1954).
2. J. C. Jaeger, *Austr. J. Phys.* **9**:167 (1956).
3. D. A. De Vries and A. J. Peck, *Austr. J. Phys.* **11**:255 (1958).
4. H. S. Carslaw and J. C. Jaeger, *Conduction of Heat in Solids* (Oxford University Press, London, 1959).
5. W. K. P. Van Loon, A. van Haneghen, and J. Schenk, *Int. J. Heat Mass Transfer* **32**:1473 (1989).

6. D. R. Chaudhary and F. Gori, *XXXIX A.T.I. Congress* (L'Aquila, Italy, II, 1984), pp. 869–874.
7. G. Grazzini, F. Gori, and T. F. Irvine, Jr., *XLIII A.T.I. Congress* (Ancona, Italy, IV, 1988), pp. 159–168.
8. D. Chaudhary, F. Gori, G. Grazzini, and A. Singh, *High Temp.-High Press.* **23**:621 (1991).
9. F. Gori and M. Pietrafesa, *ASME-WAM, HT-7A-5*, Atlanta, December 1991 or *HTD Vol. 179, Fundamental Experimental Measurements in Heat Transfer*, D. E. Beasley and J. L. S. Chen, eds., *Book N. H00663-1991* (1991), pp. 83–89.
10. F. Gori and M. Pietrafesa, *Proc. 10th Int. Heat Transfer Conf.*, Vol. 5 (Brighton, United Kingdom, 1994), pp. 349–354.
11. F. Gori, P. Coppa, and M. Pietrafesa, *Adv. Eng. Heat Transfer*, Proc. Second Baltic Heat Transfer Conf. (Southampton, 1995), pp. 101–111.
12. F. Gori, C. Marino, and M. Pietrafesa, *Int. Comm. Heat Mass Transfer* **28**:1091 (2001).
13. F. Gori and S. Corasaniti, *Proc. 5th World Conf. Experimental Heat Transfer, Fluid Mechanics and Thermodynamics,* Vol. 2 (2001), pp. 1257–1262.
14. F. Gori and P. Coppa, *Proc. ESDA 2002: 6th Biennial Conf. Eng. Systems Design and Analysis* (Instanbul, Turkey, 2002).
15. S. V. Patankar, *Numerical Heat Transfer and Fluid Flow* (Hemisphere, New York, Washington, Philadelphia, London, 1980), pp. 41–77.